Nanoscale

PAPER

View Article Online
View Journal

Cite this: DOI: 10.1039/c6nr01940d

Pressure-controlled formation of crystalline, Janus, and core–shell supraparticles†

Thomas Kister,[a] Marko Mravlak,[b] Tanja Schilling[b] and Tobias Kraus*[a]

Received 7th March 2016,
Accepted 18th June 2016

DOI: 10.1039/c6nr01940d

www.rsc.org/nanoscale

Binary mixtures of nanoparticles self-assemble in the confinement of evaporating oil droplets and form regular supraparticles. We demonstrate that moderate pressure differences on the order of 100 kPa change the particles' self-assembly behavior. Crystalline superlattices, Janus particles, and core–shell particle arrangements form in the same dispersions when changing the working pressure or the surfactant that sets the Laplace pressure inside the droplets. Molecular dynamics simulations confirm that pressure-dependent interparticle potentials affect the self-assembly route of the confined particles. Optical spectrometry, small-angle X-ray scattering and electron microscopy are used to compare experiments and simulations and confirm that the onset of self-assembly depends on particle size and pressure. The overall formation mechanism reminds of the demixing of binary alloys with different phase diagrams.

1 Introduction

Confined nanoparticles can spontaneously arrange into regular superlattices.[1–3] Binary mixtures of uniform particles thus arrange at liquid–air interfaces,[1] liquid–liquid interfaces,[3] and inside droplets.[4] Self-assembly can be explained by a combination of entropic space-filling arguments and minimization of the interparticle potentials, with relative contributions that depend on the particle core, ligand shell, solvent, and process parameters. The large parameter space leads to a remarkable structural diversity of the superstructures.[1,2] Particle films are probably the best-studied system, and they may find applications as semiconductor layers in devices.[5,6]

Less is known on particle self-assembly mechanisms inside droplets. Mixtures of particles have not yet been assembled inside emulsions, although uniform nanoparticle dispersions confined to the dispersed phase of an emulsion form well-defined clusters known as supraparticles.[4,7,8] Similar structures have been created by drying droplets on superamphiphobic surfaces.[8]

In this contribution, we study the structure of binary supraparticles that form inside emulsions. We obtained supraparticles with different structures when evaporating the droplets of an oil-in-water emulsion (Fig. 1). Supraparticles with AB_{13} superlattice structure,[1] Janus-type demixed supraparticles,[9] or core–shell particles[10] formed (Fig. 1) from the same particle mixtures depending on surfactant or external pressure. Structured particles are of interest for a range of applications: Patchy particles self-assemble into soft materials,[11] Janus particles form extremely stable Pickering emulsions,[12] and metal–oxide particles improve homogeneous (photo)catalysis,[13] for example.

Particle assembly in emulsions lends itself naturally to *in situ* observation. In contrast to superlattices that form in a highly dynamic evaporating liquid film, evaporating emulsions are easily observed *via* spectrometry. We used a combination of scattering and transmission methods to assess the formation routes of the different supraparticle geometries. A comparison with detailed molecular dynamics simulations strongly suggests that even moderate pressure differences inside the droplets change the interparticle potentials, affect the nucleation behavior, and trigger different assembly routes.

2 Experimental section

All chemicals were obtained from Sigma Aldrich (unless noted otherwise) and used without further purification.

2.1 Nanoparticle synthesis

Gold nanoparticles (AuNP) with diameters of 4 nm or 8 nm were synthesized using a modified protocol based on the original method by Wu and Zheng.[14] 8 nm nanoparticles were produced as follows. A mixture of 8 mL benzene (puriss. ≥99.7%), 8 mL oleylamine (technical grade, 70%) and 100 mg of $HAuCl_4 \cdot xH_2O$ was stirred at 20 °C and 500 rad min^{-1} for

[a]INM – Leibniz Institute for New Materials, Campus D2 2, 66123 Saarbrücken, Germany. E-mail: tobias.kraus@leibniz-inm.de; Fax: +49681 9300 279; Tel: +49681 9300 389
[b]Theory of Soft Condensed Matter, Physics and Materials Science Research Unit, Université du Luxembourg, L-1511 Luxembourg, Luxembourg

†Electronic supplementary information (ESI) available. See DOI: 10.1039/C6NR01940D

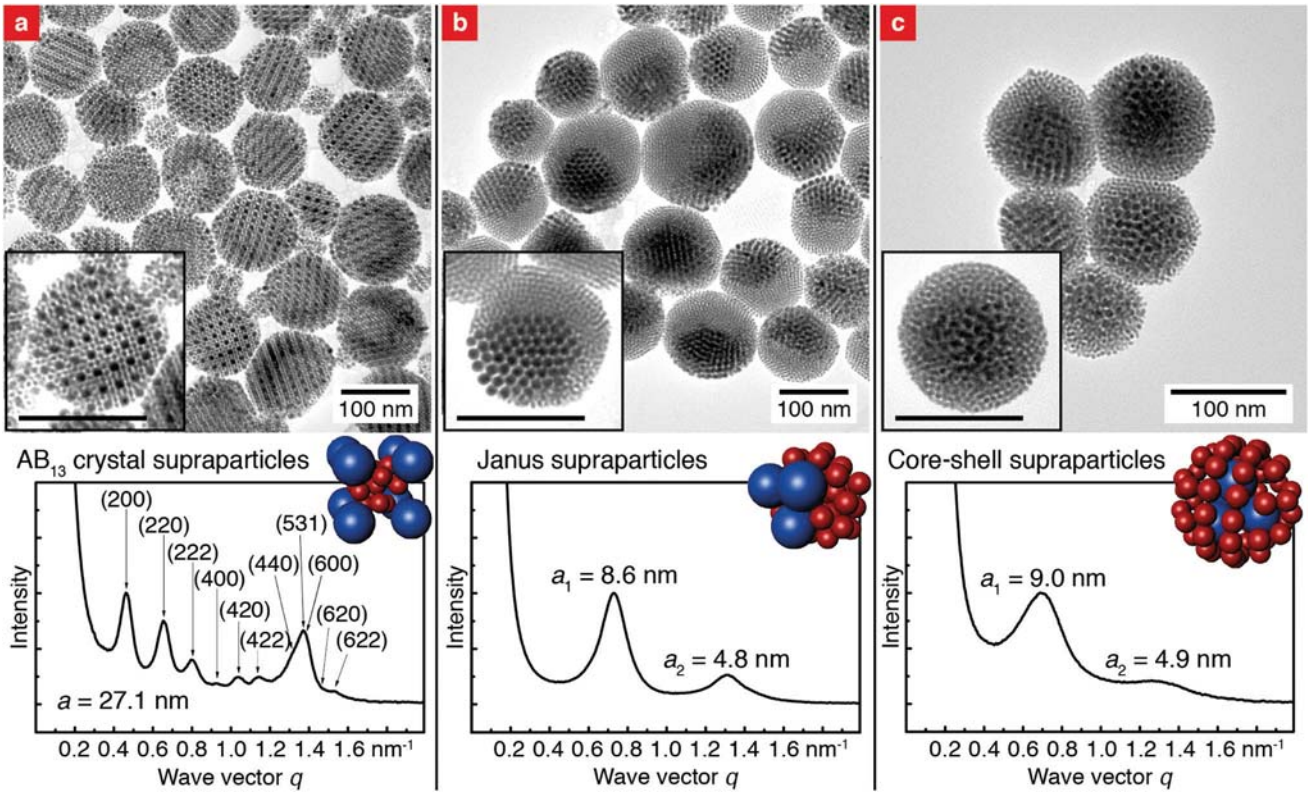

Fig. 1 Supraparticles containing hexadecanethiol-coated gold nanoparticles with diameters of 4 nm and 8 nm in a concentration ratio of 13 : 1 observed with transmission electron microscopy (TEM) and small-angle X-ray scattering (SAXS). All supraparticles were formed in hexane-in-water emulsions stabilized with different surfactants. (a) Superlattice particles formed with Triton X-100. The peaks correspond to the AB_{13} structure.[17] (b) Janus supraparticles formed with Triton X-102 or X-165. Each was composed of two pure, single nanoparticle crystals that cause distinct peaks in SAXS. (c) Core–shell supraparticles formed with Triton X-705. A crystalline core of 8 nm particles was surrounded by a random dense packing of 4 nm particles that cause a broad, shifted peak in SAXS. The supraparticle radii and dispersities for (a), (b) and (c) were 47.0 nm ± 31%, 46.2 nm ± 22% and 47.8 nm ± 26%, respectively.

1 min. Afterwards 40 mg *tert*-butylamine borane (ABCR, 97%) which was dissolved in 2 mL benzene and 2 mL oleylamine was added to the solution. The color of the solution immediately became dark purple. After stirring for 60 min at 20 °C, the nanoparticles were purified once by precipitating with 30 mL ethanol and centrifugation at 4000 rad min^{-1} for 5 min. The precipitated nanoparticles were redispersed in 20 mL heptane (puriss. ≥99%). AuNP with a diameter of 4 nm were obtained using pentane (reagent grade, 98%) instead of benzene and stirring for 30 min before adding *tert*-butylamine borane.

2.2 Nanoparticle characterization

The core size of the NPs was measured by analyzing transmission electron microscopy (TEM) micrographs taken with a JEOL JEM 2010 at 200 kV (Fig. S1 and S2 in the ESI†). A minimum of 2000 particles was counted with the ImageJ 1.45s software for each size.

2.3 Ligand exchange

The ligands of the AuNP were exchanged to make them suitable for supraparticle formation.

Oleylamine-stabilized AuNP from above were heated to 80 °C under argon. A solution of triphenylphospine (≥98.5% GC, 5 times the amount of gold) in heptane was also heated to 80 °C and added to the AuNP. After stirring for 60 s, the color of the solution turned from dark purple to dark blue and finally to black, indicating agglomeration. Upon addition of 1-hexadecanethiol (≥95.0% GC, 10 times the amount of gold), the solution immediately returned to purple, indicating de-agglomeration. The mixture was stirred at 80 °C for 10 min. The resulting particles were purified once by precipitation with ethanol and centrifugation and resuspended in hexane (CHROMASOLV ≥ 95%).

2.4 Supraparticle synthesis

All supraparticles contained AuNP with core diameters of 4 nm and 8 nm.

To prepare supraparticles, 16 mL of ultrapure water containing a surfactant[15] (Triton X-100 (laboratory grade), X-102 (Dow Chemical, 100%), X-165 (Dow Chemical, 70%), X-305 (Dow Chemical, 70%), X-405 (Dow Chemical, 70%), X-705 (Dow Chemical, 70%), or sodium dodecyl sulfate (≥98.0% GC), concentrations listed in Table 1) and 320 μL of hexane with AuNP

Table 1 Concentration of the surfactants in the water phase and the corresponding critical micelle concentrations

Surfactant	Concentration [g L^{-1}]	CMC [g L^{-1}]
X-100	9.45	0.189
X-102	13.4	0.267
X-165	28.5	0.570
X-305	19.2	1.92
X-405	24.4	2.44
X-705	35.9	3.59

carrying 1-hexadecanethiol ligand shells were stirred with an Ultra-Turrax (Janke Kunkel, T25 S5) shear emulsifier at 20 000 rad min^{-1} for 30 min. The resulting hexane-in-water emulsion was heated to 50 °C for 12 h in an open vessel. Upon evaporation of the hexane the nanoparticles arranged into supraparticles.[4]

2.5 Supraparticle characterization

The structure of the supraparticles was analyzed by TEM (JEOL JEM 2010 at 200 kV) and small angle X-ray scattering (SAXS) in a Xeuss 2.0 (Xenocs SA, Grenoble, France) setup equipped with a copper Kα (λ = 0.154 nm) X-ray source and a Hybrid Photon Counting detector (PILATUS 1M, DECTRIS, Baden, Switzerland). Sample to detector distance was capped between 1240 mm and 2500 mm.

The size of the supraparticles was measured from the dynamic light scattering (DLS) at 90 degree using a Wyatt Technology DynaPro Titan with a laser wavelength of 831.2 nm. The dispersity (indicated after the respective mean radius) is defined as the ratio of standard deviation and mean radius. The evaluated regularization expansion of the autocorrelation was fitted with the Dynals algorithm (supplied by Alango).

The supraparticles were washed twice for TEM analysis (centrifugation at 500 rcf for 20 min, removing supernatant and redispersing with clear water) to remove the excess surfactant. Small angle X-ray scattering showed no effect of the washing steps on the supraparticles' structure.

2.6 Pendant drop tensiometry

Interfacial tensions were measured using the pendant drop method in an OCA 35 (Dataphysics, Neuhausen, Germany) setup. An aqueous solution of the surfactant in question with the concentration used in the emulsion was held in a glass cuvette. Pure hexane was injected from a J-shaped cannula until a drop formed. The volume of the drop was adjusted to almost detach from the cannula. The shape of the pendant drop was recorded by a digital camera until the drop reached equilibrium. The final shape was fitted with the Young–Laplace equation to calculate interfacial tension. The arithmetic mean and the standard deviation were calculated from a minimum of 200 calculated tension values obtained in the equilibrium state.[16] The measurements were performed at 25 °C and 50 °C.

2.7 Pressure dependent experiments

A pressure chamber (type: Drifton 25-DY, Drifton, 2650 Hvidovre, Denmark) was used to produce supraparticles under external hydrostatic pressure. Freshly prepared emulsion was placed into an open vessel inside the chamber. Excess pressure was applied by filling the headspace with compressed nitrogen. A mechanical manometer indicated the pressure inside the chamber.

Pressure-dependent *in situ* SAXS measurements were performed in a capillary with two open ends. A valve was mounted at the output of the capillary to close the channel after the sample had been introduced. A syringe pump (Nemesys) held a gas-tight glass syringe that we connected to the open end of the capillary to apply pressure. An electronic pressure sensor was mounted between the syringe pump and the flow capillary to monitor the applied pressure.

3 Results and discussion

Hexane-in-water emulsions were prepared with nanoparticles in the oil phase and non-ionic surfactants (octylphenol ethoxylates, trade name 'Triton') with hydrophilic tails of varying molecular weights in the aqueous phase. We mainly used hexane for its conveniently low boiling point, but heptane or toluene led to similar results (not shown here).

The nanoparticles had gold cores with diameters of 4 nm and 8 nm and narrow size distributions with relative standard deviations of the diameter between 5 and 7%. They were coated with hexadecanethiol self-assembled monolayers that made them dispersible in hexane but incompatible with water. The particle concentrations were 3.9×10^{15} mL^{-1} and 3×10^{14} mL^{-1} for 4 nm and 8 nm, respectively.

Supraparticles were formed by gently evaporating the oil phase at 50 °C. Hexane slowly evaporated from the emulsion until the droplets had shrunk from their initial diameter of 2 μm to an average of 150 nm. Typical standard deviations were around 15% to 20% as measured by dynamic light scattering.

During evaporation, the nanoparticle mixtures in the droplets arranged into regular structures. Fig. 1a shows supraparticles that remind of $NaZn_{13}$, a phase that has been reported for nanoparticle superlattices in thin films.[1] The AB_{13} lattice appears to be almost undisturbed even in small supraparticles. This is in contrast to supraparticles consisting of only one particle size, which deviate from close packing and exhibit lower-symmetry geometries known from atomic clusters.[4]

AB_{13} supraparticles only formed with Triton X-100 (Fig. 1a). Surfactants with longer hydrophilic tails such as Triton X-102 and X-165 led to the formation of Janus-type supraparticles composed of two 'pure' supercrystals of nanoparticles each (Fig. 1b). The surfactants with the longest hydrophilic chains, Triton X-305, X-405, and X-705, gave rise to core–shell supraparticles in which a crystalline core of large nanoparticles was surrounded by a randomly packed shell of smaller nanoparticles (Fig. 1c).

Different formation mechanisms could be evoked to explain the surfactant-dependent structure of the supraparticles. Marangoni flows can separate nanoparticles with different sizes in sessile drops.[18,19] Such flows are characterized by the Marangoni number Ma ≡ /dσ/dT/ΔTR/(ηα), where dσ/dT is the change of the interfacial tension with temperature, ΔT is a temperature difference, R the radius of the droplet, a the dynamic viscosity and α the thermal diffusivity. An upper bound for Ma for hexane as used in our experiments is 5, far below the critical number of 80 reported for the onset of Marangoni flows,[19] which excludes Marangoni flows as an explanation for the formation of different supraparticles.

Pickering-Ramsden emulsions with nanoparticles trapped at the liquid–liquid interfaces[20,21] can also be excluded as structure-directing mechanism. Alkanethiol-coated gold nanoparticles with 6 nm diameter do not segregate to hexane–water interfaces with Triton X-100.[16] Likewise, interfacial tension measurements that we performed indicated no segregation for any of the surfactants that we used here.

We believe that the formation of supraparticles is dominated by nucleation: different supraparticles form when self-assembly starts at different particle concentrations. Dispersibility sets an upper critical concentration for agglomeration (in the following, we call all processes that lead to dense particle packings 'agglomeration', regardless of whether the particles self-assemble into regular lattices or form amorphous structures). If dispersibility is high (for repulsive interparticle potentials), agglomeration occurs late in the evaporation process, when high particle concentrations are reached. If it is low (for attractive interparticle potentials), agglomeration occurs earlier, at lower particle concentrations.

Fig. 2a shows the formation of AB_{13} supraparticles in emulsions stabilized by Triton X-100 (with an average of 9 to 10 ethoxylate units as hydrophilic chain). First changes became visible after 150 min; an AB_{13} structure formed after 180 min. Further evaporation did not change the structure, but the lattice spacing decreased as indicated by peak shifts.

Now consider the evaporation of emulsions stabilized by Triton X-165 (with an average of 16 ethoxylate units as hydrophilic chain) shown in Fig. 2b: after 240 min of evaporation, the larger nanoparticles started to agglomerate, as indicated by a peak in SAXS. After 420 min, a second peak indicated the agglomeration of the smaller particles that have a larger critical concentration. Large particles agglomerate first because they attract each other more strongly than smaller particles.[22] The smaller particles agglomerate in a separate crystal later, and both are joined into a Janus supraparticle by the shrinking droplet.

The onset of self-assembly was shifted to even larger concentrations when using Triton X-705 (with an average of 55 ethoxylate units) as shown in Fig. 2c. Agglomeration of the larger particles set in after 270 min, and the smaller nanoparticles did not agglomerate until an abrupt transition after 660 min. At this point, there was little free volume left; the small particles arranged into a shell around the existing crystal of large particles and formed a core–shell supraparticle.

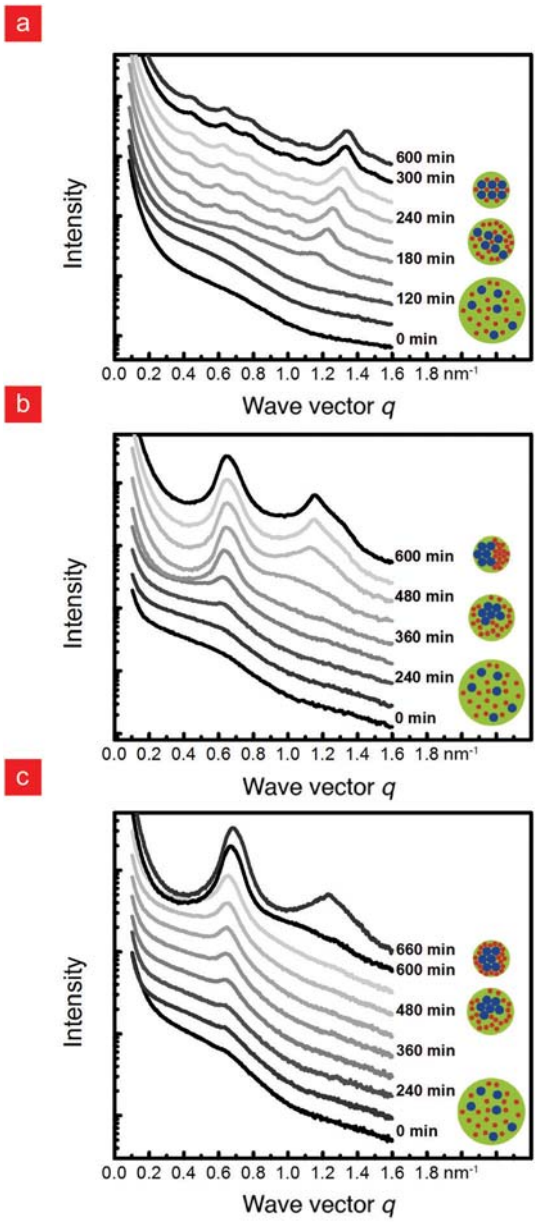

Fig. 2 (a) Evaporation of a Triton X-100 stabilized emulsion. Minor changes became visible after 150 min of evaporation. A clear AB_{13} superlattice formed after 180 min. (b) Evaporation of a Triton X-165 stabilized emulsion. After 240 min of evaporation, the larger particles began to agglomerate and caused a broad SAXS peak. Upon prolonged evaporation, the larger nanoparticles agglomerated further, followed by agglomeration of the smaller particles after an additional 200 min. Further increase of confinement compressed the agglomerates and shifted the peaks. (c) SAXS observation of the evaporation of a particle-containing emulsion stabilized with Triton X-705 at larger Laplace pressure. After 270 min of evaporation, the larger particles began to agglomerate. The smaller particles remained dispersed much longer than for Triton X-165 and abruptly agglomerated in the end.

In contrast, particles in emulsion droplets stabilized with Triton X-100 (with an average of 9.5 ethoxylate units) agglomerated at a critical concentration that was reached long before all

hexane had evaporated, much earlier than for X-165 and X-705. This is readily explained if we assume a stronger attraction between nanoparticles in droplets with Triton X-100 than between nanoparticles in droplets with Triton X-165.

We performed molecular dynamics simulations[23] to test which interaction potentials between nanoparticles lead to the observed structures. Disordered binary mixtures of 7000–14 000 nanoparticles were confined in a hard spherical container and then left to equilibrate. The self-assembly of particles with a purely repulsive Weeks–Chandler–Andersen (WCA) pair potential[24] was compared to particles with a more attractive Lennard-Jones potential. Intermediate cases were modeled by linearly superimposing the potentials.

Fig. 3a–c shows the final configurations for different interaction potentials. Purely repulsive particles that were confined at high concentrations to a container with fixed volume readily arranged into AB_{13} crystals. This is in agreement with previous studies.[17,25] Adding identical attraction to all particles (regardless of their size) in the same container led to AB_{13} crystals, too.

Simulations in shrinking containers emulate the effect of droplet evaporation. When we added attractive interactions only to the large particles in a mixture that we confined to a shrinking container, core–shell supraparticles formed. This models cases where the van der Waals attraction between larger particles dominates agglomeration.[22] When we added attractive interactions to both particle types, Janus supraparticles formed. Fig. 3d shows the formation stages of a Janus supraparticle: separate agglomerates of the larger particles nucleated and merged, while the smaller particles remained disordered. Crystallization of the smaller particles occurred at a later stage. This is consistent with our assembly model and the SAXS data presented above: larger particles exhibit stronger attractive interactions than smaller particles with the same ligand molecules.

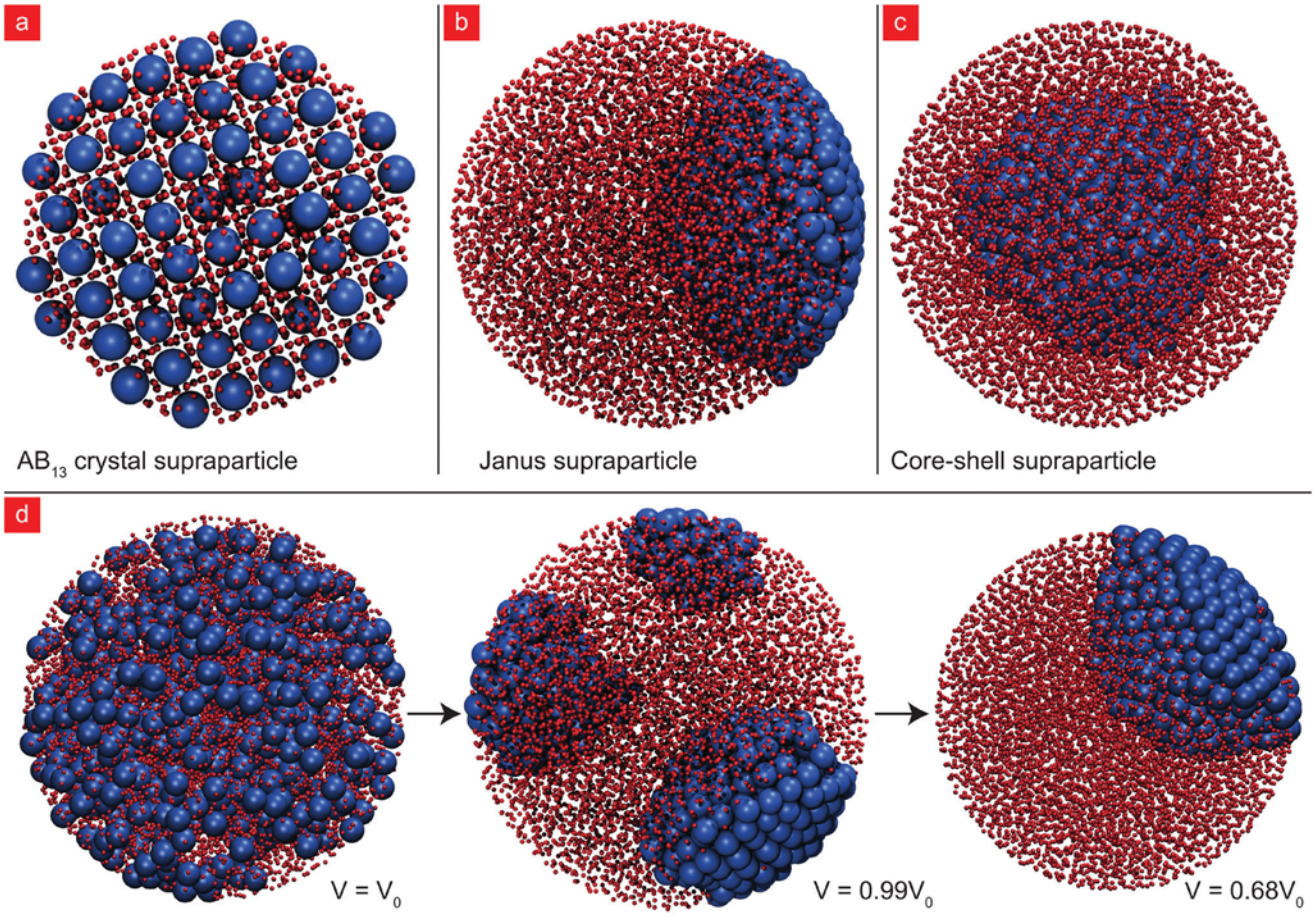

Fig. 3 Molecular dynamic simulations of nanoparticles confined in a spherical container that shrank during the simulation (with the exception of panel (a)). (a) AB_{13}-structured supraparticles with entropically dominated structures formed with purely repulsive particle interactions that approximate the high pressure regime. The same AB_{13} lattice also formed when all particles attracted each other, as in the low pressure experiments. (b) Weak interactions between the larger nanoparticles led to a core–shell structure. (c) Attractions that scale with particle size led to Janus particles. (d) Snapshots of the formation of a Janus supraparticle in a shrinking container. The left image shows the fully dispersed state just before agglomeration occurred. The larger particles agglomerated slowly in different parts of the volume, moving in between the disordered smaller particles. The agglomerates then joined to form a crystal at one side of the volume. Finally, the smaller particles crystallized in the remaining volume. The volume change between the first agglomeration events and the fully arranged state is approximately 30%.

But how do the emulsion surfactants change the potentials between nanoparticles inside the droplets? The members of the Triton class of surfactants differ solely in the length of their polyethylene glycol chains. It is highly unlikely that chemical interactions with the liquid–liquid interface can change the interactions between particles inside the oil droplets. The experiments that we discuss below strongly suggest that *pressure* links surfactant and particle interactions. Detailed molecular-scale studies will be required to reveal the precise mechanism that may be connected to the solubility of water in the oil and the arrangement of the ligand shell.

The pressure inside an emulsion droplet of radius r depends on the interfacial tension γ of the liquid–liquid interface through the Laplace pressure, $\Delta p_L = 2\gamma/r$.[26] The interfacial tension, in turn, depends on the surfactant. We measured γ of the hexane–water interface for different surfactants by tensiometry on macroscopic drops at concentrations above the critical micelle concentration (CMC) (Fig. 4a). The results imply that droplets with a diameter of 150 nm (the average final size of the evaporating droplets) have Laplace pressures between 10 kPa for Triton X-100 and 300 kPa for Triton X-705.

The supraparticle structure depended on interfacial tension but not on the exact chemical nature of the surfactant. For example, the anionic surfactant sodium dodecyl sulfate (SDS) produced Janus-type supraparticles just as Triton X-165. This suggests that it is the Laplace pressure that affects interparticle potential and thus, supraparticle formation.

Pressure affects the dispersibility of nanoparticles in supercritical fluids. Korgel demonstrated that the critical concentration for the agglomeration of alkylthiol-stabilized gold nanoparticles in supercritical ethane increases with pressure.[27] When we applied *external* isostatic pressure to particle-laden emulsions, SAXS indicated pressure-dependent dispersibility (Fig. 4b), too: agglomerates of the larger particles dissolved when we increased the pressure and formed when we lowered it. The transition was reversible and fast; agglomerates decomposed in seconds. Small particles were consistently more soluble than big particles, probably due to the size dependence of van der Waals attraction.[22] We conclude that pressure reduces the attractive interactions between particles.

To test our hypothesis, we emulated the effect of Laplace pressure by applying external isostatic pressure on evaporating emulsions stabilized with Triton X-100 (Fig. 5a–d). AB_{13} superlattices formed at environmental pressure. Janus supraparticles formed at an external pressure of 100 kPa, and core–shell supraparticles at 300 kPa, respectively. The pressures necessary to 'switch' between different supraparticle structures were comparable to the differences in Laplace pressure caused by different surfactants.

The core–shell structures formed at 300 kPa of external pressure had cores with a higher degree of crystalline perfection than supraparticles formed with Triton X-705. The reason is probably the dependence of Laplace pressure on droplet size. When an emulsion stabilized with Triton X-705 evaporates, droplets shrink and the Laplace pressure strongly changes with time. Interactions between particles change continuously and perturb assembly. In contrast, external pressure is independent of droplet size, and crystallization is less perturbed.

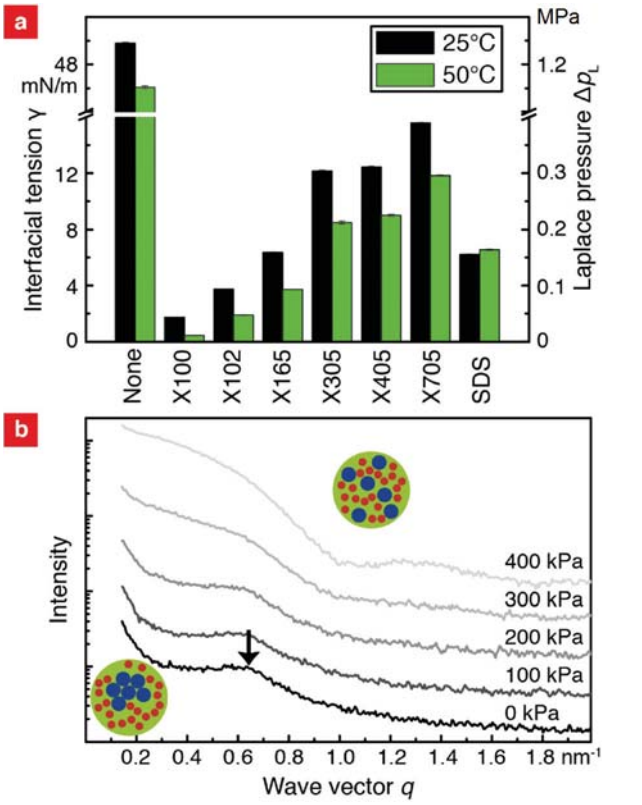

Fig. 4 (a) The pressure inside emulsion droplets depends on the surfactant. Hanging droplet tensiometry indicates the interfacial tensions between *n*-hexane and water with different surfactants at 25 and 50 °C. The right axis indicates the calculated Laplace pressure that acted on the particles in a droplet with a radius of 80 nm for the respective surfactant. (b) Pressure-dependent SAXS of particle-containing emulsions stabilized with Triton X-165 proves the pressure-dependent dispersibility of nanoparticles. The emulsion was partially evaporated for 240 min at 50 °C and ambient pressure. After this time the larger nanoparticles began to agglomerate (SAXS peak is indicated by an arrow). Upon applying external isostatic pressure on the partially evaporated emulsion, the agglomerates rapidly dissolved, and the peak was replaced by the characteristic Porod rise towards large q that indicates dispersion.

Surprisingly, the low-density AB_{13} structure (28% volume fraction of cores) gradually returned in the supraparticles when increasing external pressure up to 1000 kPa (Fig. 5c and d). The external pressure required to return to AB_{13} was larger for Triton X-100 than for Triton X-165 or X-705. Janus and core–shell supraparticles had a packing fraction above 40% (see ESI†). This excludes simple space-filling arguments as an explanation for the pressure-dependent supraparticle structure. The effects of external pressure on supraparticle structure can only be explained by pressure-dependent particle–particle interactions that change the sequence of nanoparticle agglomeration during solvent evaporation.

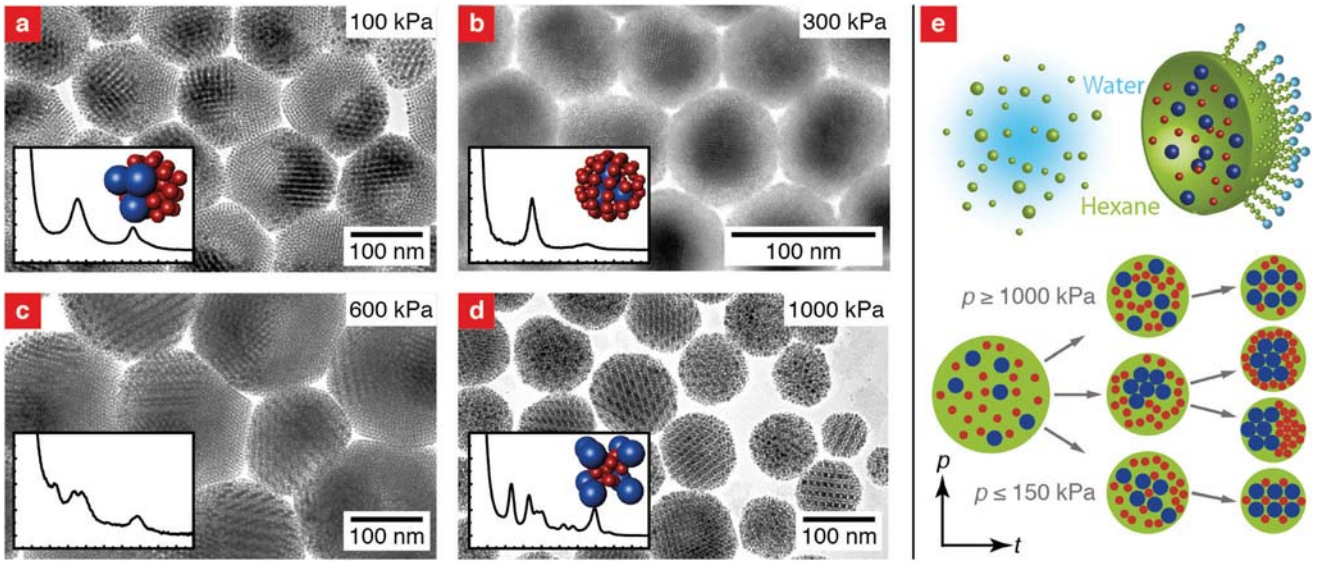

Fig. 5 Supraparticles formed in emulsions stabilized by Triton X-100, with external pressure applied. (a) 100 kPa isostatic external pressure yielded Janus supraparticles, (b) 300 kPa yielded core–shell supraparticles. (c) At 600 kPa, supraparticles with partial AB_{13} and Janus formed, and at (d) 1000 kPa, the entire supraparticles had AB_{13} structures. Inserts show the respective SAXS data. (e) Proposed formation mechanisms of the supraparticles. If the pressure inside an emulsion droplet is low, agglomeration happens early and supraparticles form *via* nucleation-and-growth. If it is high, particles remain dispersed and confinement causes late supraparticle formation. Intermediate pressures lead to intermediate situations due to the different dispersibility of large and small nanoparticles. The supraparticle radii and dispersities for (a), (b), (c) and (d) were 53.4 nm ± 26%, 119.5 nm ± 30%, 87.4 nm ± 18% and 44.8 nm ± 22%, respectively.

A formation mechanism based on a combination of agglomeration and confinement sketched in Fig. 5e explains the observations. Some of the processes described below are akin to the formation of Janus particles in flame spray pyrolysis, where a mixed phase decomposes into a solid and a liquid that solidifies later.[28]

At low pressures, agglomeration occurs long before all hexane has evaporated, and AB_{13} forms. At high pressures, dispersibility is increased, and the particles remain dispersed until almost all hexane has evaporated. The AB_{13} lattice then forms due to confinement. At intermediate pressures, the larger particles agglomerate at high particle concentrations, when little hexane remains. Low solvent content reduces the spacing between particles and inhibits relative particle motion. The particles' mobility is insufficient to reach the complex AB_{13} arrangement. Instead, the smaller particles agglomerate into single crystals, and Janus supraparticles form. A narrow range of pressures exists where agglomeration of the large particles is possible, but the smaller particles remain dispersed until almost all hexane has evaporated. This situation leads to core–shell supraparticles: confinement holds a disordered shell of small particles around the previously formed core of larger particles.

The particle–particle interactions depended on the type of ligand used. Particles with dodecanethiol required higher pressures to form Janus or core–shell structures than particles with hexadecanethiol. Shorter ligands probably cause increased attraction between the particles[29] that has to be reduced by pressure to arrive at the levels required for self-assembly.

4 Conclusions

We showed that nanoparticles can arrange into binary crystalline structure inside evaporating emulsion droplets. Furthermore, we demonstrated that pressure can be used to manipulate the interactions of nanoparticles and thus, the overall structure of the supraparticles.

The binary supraparticles that we introduce here are an interesting new class of structured particles. In contrast to diblock copolymer particles,[30] they contain inorganic cores. Such cores are available with magnetic, plasmonic, fluorescent, catalytic and many other properties. Supraparticles combine them in a well-defined configuration.

Pressure is a simple and convenient stimulus to define supraparticle structure. Moderate pressure changes have surprisingly large effects on dispersibility and structure. It remains to be seen whether nanoparticle self-assembly in liquid films (often used to create superlattices) is also affected by pressure.

Molecular-scale studies of the ligand shell will give insight on the mechanism that causes the pressure-dependent interaction potentials. The pressure-dependent stability of alkanethiol-coated nanoparticle probably stems from the solvation of the ligand shell by the solvent.[27] We expect that other nanoparticle types that can be also coated with alkane ligands (if necessary, using linker chemistries other than thiols) can also be arranged in supraparticles using our route. This will allow to combine plasmonic metal particles, catalytic oxide particles, and fluorescent semiconductor quantum dots into structured

particles with new functionalities that are due to energy exchange between the constituent particles. Sintering such supraparticles will lead to new alloy particles that are impossible to create by direct synthesis.

Recent results suggest that particle agglomerates retain some mobility depending on the ligand shells.[31] Pressure-induced structural changes may also be possible in the fully formed supraparticles. Such active supraparticles could provide pressure-sensitive properties for externally controlled self-assembly.

Acknowledgements

We thank A. Kleemann for technical support during synthesis and L. González-García for 3D illustrations. This work was financial supported by the DFG – Deutsche Forschungsgemeinschaft – and the Luxembourgish Fonds National de la Recherche (FNR). We thank E. Arzt for his continuing support of this project.

References

1 E. V. Shevchenko, D. V. Talapin, N. A. Kotov, S. O'Brien and C. B. Murray, *Nature*, 2006, **439**, 55–59.
2 W. H. Evers, B. D. Nijs, L. Filion, S. Castillo, M. Dijkstra and D. Vanmaekelbergh, *Nano Lett.*, 2010, **10**, 4235–4241.
3 O. Velev, K. Furusawa and K. Nagayama, *Langmuir*, 1996, **12**, 2385–2391.
4 J. Lacava, P. Born and T. Kraus, *Nano Lett.*, 2012, **12**, 3279–3282.
5 Z. Nie, A. Petukhova and E. Kumacheva, *Nat. Nanotechnol.*, 2010, **5**, 15–25.
6 K. Whitham, J. Yang, B. H. Savitzky, L. F. Kourkoutis, F. Wise and T. Hanrath, *Nat. Mater.*, 2016, **15**(5), 557–563.
7 B. de Nijs, S. Dussi, F. Smallenburg, J. D. Meeldijk, D. J. Groenendijk, L. Filion, A. Imhof, A. van Blaaderen and M. Dijkstra, *Nat. Mater.*, 2015, **14**, 56–60.
8 S. Wooh, H. Huesmann, M. N. Tahir, M. Paven, K. Wichmann, D. Vollmer, W. Tremel, P. Papadopoulos and H.-J. Butt, *Adv. Mater.*, 2015, **27**, 7338–7343.
9 S.-H. Hu and X. Gao, *J. Am. Chem. Soc.*, 2010, **132**, 7234–7237.
10 O. Chen, L. Riedemann, F. Etoc, H. Herrmann, M. Coppey, M. Barch, C. T. Farrar, J. Zhao, O. T. Bruns, H. Wei, P. Guo, J. Cui, R. Jensen, Y. Chen, D. K. Harris, J. M. Cordero, Z. Wang, A. Jasanoff, D. Fukumura, R. Reimer, M. Dahan, R. K. Jain and M. G. Bawendi, *Nat. Commun.*, 2014, **5**, 5093.
11 S. C. Glotzer and M. J. Solomon, *Nat. Mater.*, 2007, **6**, 557–562.
12 M. Lattuada and T. A. Hatton, *Nano Today*, 2011, **6**, 286–308.
13 M. R. Hoffmann, S. T. Martin, W. Choi and D. W. Bahnemann, *Chem. Rev.*, 1995, **95**, 69–96.
14 B.-H. Wu, H.-Y. Yang, H.-Q. Huang, G.-X. Chen and N.-F. Zheng, *Chin. Chem. Lett.*, 2013, **24**, 457–462.
15 T. D. C. Company, *Technical Data Sheet*, Triton, http://www.dow.com, 2015.
16 J. Lacava, A.-A. Ouali, B. Raillard and T. Kraus, *Soft Matter*, 2014, **10**, 1696–1704.
17 A. Schofield, P. Pusey and P. Radcliffe, *Phys. Rev. E: Stat. Phys., Plasmas, Fluids, Relat. Interdiscip. Top.*, 2005, **72**, 031407.
18 E. Hendarto and Y. B. Gianchandani, *J. Micromech. Microeng.*, 2013, **23**, 075016.
19 J. J. Hegseth, N. Rashidnia and A. Chai, *Phys. Rev. E: Stat. Phys., Plasmas, Fluids, Relat. Interdiscip. Top.*, 1996, **54**, 1640–1644.
20 V. N. Manoharan, M. T. Elsesser and D. J. Pine, *Science*, 2003, **301**, 483–487.
21 W. Ramsden, *Proc. R. Soc. A*, 1903, 156–164.
22 V. A. Parsegian, *van der Waals forces: a handbook for biologists, chemists, engineers, and physicists*, Cambridge University Press, New York, 2005.
23 S. Plimpton, *J. Comput. Phys.*, 1995, **117**, 1–19.
24 J. D. Weeks, D. Chandler and H. C. Andersen, *J. Chem. Phys.*, 1971, **54**, 5237–5247.
25 M. Eldridge, P. Madden and D. Frenkel, *Nature*, 1993, **365**, 35–37.
26 F. Menger, *J. Phys. Chem.*, 1979, **83**, 893–893.
27 P. S. Shah, J. D. Holmes, K. P. Johnston and B. A. Korgel, *J. Phys. Chem. B*, 2002, **106**, 2545–2551.
28 G. A. Sotiriou, A. M. Hirt, P.-Y. Lozach, A. Teleki, F. Krumeich and S. E. Pratsinis, *Chem. Mater.*, 2011, **23**, 1985–1992.
29 S. J. Khan, F. Pierce, C. Sorensen and A. Chakrabarti, *Langmuir*, 2009, **25**, 13861–13868.
30 M. A. C. Stuart, W. T. Huck, J. Genzer, M. Müller, C. Ober, M. Stamm, G. B. Sukhorukov, I. Szleifer, V. V. Tsukruk, M. Urban, F. Winnik, S. Zauscher, I. Luzinov and S. Minko, *Nat. Mater.*, 2010, **9**, 101–113.
31 T. Geyer, P. Born and T. Kraus, *Phys. Rev. Lett.*, 2012, **109**, 128302.

